IEEE Robotics and Automation Letters (RAL) paper presented at
2024 IEEE/RSJ International Conference on Intelligent Robots and Systems (IROS)
October 14-18, 2024. Abu Dhabi, UAE

A Novel Miniature Flexible Instrument with Unfolding and Decoupling Design for Endoscopic Surgery

Chi Zhang, Yi Wang, Tao Liang, Kang Kong, Qiwen Yao and Siyang Zuo*

***Abstract*— Nowadays, gastrointestinal cancer has widely impacted people's health worldwide due to its high mortality rate. Early treatment of gastrointestinal cancer by endoscopic procedure can greatly increase survival rates of patients. Nevertheless, current flexible endoscopic instruments lack of degree of freedom and surgical triangulation, thereby presenting challenges in the execution of endoscopic procedures. To solve these problems, this paper proposes a novel miniature dual-bending flexible instrument with an outer diameter of 2.8 mm and a length of 1100 mm, which is compatible with commercial endoscope and various endoscopic platforms. Discrete frame stacking structure with unfolding and decoupling design empowers the instrument to achieve high flexibility, accurate bending motions and surgical triangulation. The flexible instrument can achieve a large hemi-spherical workspace with a radius of 24 mm without considering linear movement. The measured tip positioning accuracy is better than 0.59 mm for wrist bending motion. Combined with the various end effectors, the instrument can perform complex endoscopic procedures facilitated by the master-slave control method. Through *in-vivo* animal experiments, the clinical potential and practicality of the instrument have been demonstrated.**

***Index Terms*—Flexible instrument, gastrointestinal cancer, endoscopic surgery, ESD, continuum structure.**

I. INTRODUCTION

GASTROINTESTINAL (GI) cancer is gradually becoming high incidence worldwide, including esophageal cancer, gastric cancer, colorectal cancer, etc. The high incidence and low diagnosis rate of this type of cancer have serious implications for human health. According to the "Global Cancer Report" released by the World Health Organization in 2018 [1], gastric cancer, one of the gastrointestinal cancers, accounts for 5.7% of all cancer cases and ranks fifth. Due to the low diagnosis rate of gastrointestinal cancer, people often lose the best time for timely treatment because they discover the cancer too late. According to clinical practice, the depth of invasion of early malignant tumors is limited to the mucosal layer or exceeds the submucosal layer. If it can be diagnosis and treatment early, it can effectively improve the five-year survival rate of patients, reaching a level of 90 %. However, for advanced gastric cancer patients, this data is only 10 % [2]. Endoscopic surgery based on flexible instruments can effectively avoid complications and has advantages such as low anesthesia requirements and mild pain [3]. Endoscopic submucosal dissection (ESD) is a typical gastrointestinal surgery and has become an ideal treatment option for the diagnosis and treatment of early-stage gastrointestinal cancers. However, current endoscopic instruments lack of degree of freedom (DOF). And the channels and camera of the endoscope are in close, making the loss of the surgical triangulation. These problems will increase the technical challenges in the endoscopic procedure. In recent years, multi-DOF flexible instruments applied to endoscopic surgery have been extensively studied and developed.

Kato et al. [4] proposed a flexible instrument driven by steel wire, with an overall outer diameter of 3.4 mm and a main body fabricated by laser-cutting of superelastic nickel-titanium alloy tube. Through the design of two segments near the proximal and distal ends, the instrument can achieve an S-shaped bend. Ping et al. [5] proposed a nickel-titanium alloy flexible continuous scanner based on a contact-assisted flexible mechanism. It has good positioning accuracy and resistance to tensile and torsional forces. Gao et al. [6] proposed a two-dimensional (2-D) asymmetric flexible catheter to render two different bending characteristics to adapt to the special anatomy. The contact-aided compliant mechanism is adopted by designing the asymmetric blocks to form the self-collision in one lateral bending direction. However, these flexible hinge designs are difficult to achieve double-bending, and has problems of easy rupture of the flexible hinge parts, and complicated wire guiding structure.

Discrete backbone structure is frequently used in the design of flexible surgical instruments. Andreas et al. [7] proposed a 6 DOFs flexible surgical instrument, which consists of a multi-DOF bending section made up of short rigid joints with an outer diameter of 4 mm. Seow et al. [8] developed a flexible robotic arm, which is composed of 18 joints units with a length of 32.5 mm. Each pair of adjacent joint units is connected by a spherical joint, and the entire instrument is driven by two sets of driven wires to achieve two DOFs for bending. Meer et al. [9] and Harada et al. [10] used similar spherical joint structures in the design of the flexible bending section of their instruments. Hong et al. [11] proposed a 5 DOFs flexible surgical instrument. The outer diameter is 3 mm, and it is composed of rigid joints made from multiple

Manuscript received: July 8, 2023; Revised: September 16, 2023; Accepted: November 19, 2023. This paper was recommended for publication by Editor Xinyu Liu upon evaluation of the Associate Editor and Reviewers' comments. This work was supported by the National Natural Science Foundation of China under Grant 62133010. (Corresponding author: Siyang Zuo.)

C. Zhang, Yi Wang, T Liang, K Kong, Qiwen Yao, and *S. Zuo are with Key Laboratory of Mechanism Theory and Equipment Design of Ministry of Education, Tianjin University, Tianjin, CO 300072 China (e-mail: siyang_zuo@tju.edu.cn).

Digital Object Identifier (DOI): see top of this page.

metal 3D printing layers. The joints are connected by involute gears, which increase the stability of joint contacts. However, due to the relatively long length of the joints, the flexibility of the instrument is poor. Imperial College London [12] developed a 5 DOFs wire-driven flexible instrument. The outer diameter is 4.5mm, and the connection between adjacent connecting rods in the wrist structure adopts a triangular-circular backbone design to reduce friction during joint rotation. The above-mentioned flexible instruments based on a discrete backbone structure increases the life and practicality of the instrument. It achieves miniaturization design and multi-DOF motion. However, in the general form of backbone stacking, the bending angle of a single joint is too large, and as the DOF increases, the flexibility of the instrument's movement decreases significantly. In the redundant drive discrete backbone structure, the number of the instrument's DOF is often limited. Although the flexibility of the instrument can be increased by arranging multiple segments of bending, the layout of the driven wire still easily causes motion coupling between different segments of bending.

In view of the limitations of current flexible endoscopic instruments, this paper proposes a dual-bending design for flexible instrument based on a discrete frame stacking structure. It allows for the realization of the surgical triangulation in endoscopic surgery. The main novelty and contribution of this work are as follows:

(1) A 7 DOFs flexible forceps and 6 DOFs flexible electric knife have been developed, with an outer diameter of only 2.8mm and an insertion length of 1100mm. It can be adopted to commercial GI endoscope and various endoscopic platforms.

(2) A 2 DOFs unfolding structural design scheme capable of forming the surgical triangulation has been proposed. The unfolding structure and the wrist bending part are decoupled based on symmetrical design.

(3) A curved cylindrical sliding contact frame has been designed, which makes the displacement changes of the driven wires in symmetrical positions approximately equal, providing better flexibility for the instrument's motion.

II. Method

A. Overall Structure Design

To meet the requirements for endoscopic surgery, a flexible instrument has been designed to accommodate various end effectors (mainly surgical forceps and high-frequency electrosurgical knife). The overall structure is shown in Fig. 1(a).

The flexible instrument is composed of active bending part, passive bending part and end effector. The active bending part consists of 17 rigid frames, including 4 fixed frames (blue frames in Fig.1) and 13 transitional frames (red frames in Fig.1). The entire flexible bending part has a length of 32.4 mm, an outer diameter of 2.8 mm, and an inner diameter of 1.2 mm. The section view of wrist bending frame is shown in Fig. 1(b), with through-hole of 0.3 mm in diameter processed on the frame tube wall to transmit the driven wire. And section view of the shoulder bending frame is shown in Fig. 1(c), with four more driven wire holes for decoupling wires. Specific parameters are summarized in Table I. The prototype of the instrument is shown in Fig. 1(e). High-density polyethylene (HDPE) is selected as the material for the passive bending part due to its non-toxic, odorless, good acid and alkali resistance, organic solvent resistance, and electrical insulation properties [13].

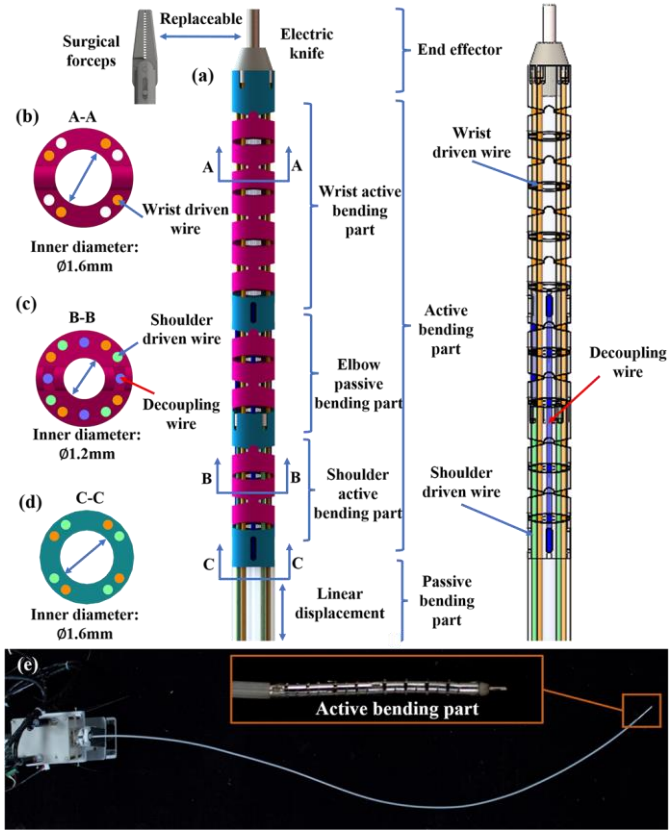

Fig. 1. Structure of the instrument. (a) Overall design of the flexible instrument. (b) Section view of the wrist bending frame. (c) Section view of the shoulder bending frame. (d) Section view of the passive bending part. (e) Prototype of the instrument.

The section view of passive bending part is shown in Fig. 1(d). The passive bending part is 2.8 mm in outer diameter, 1.6 mm in inner diameter, and there are 8 driven wire channels with a diameter of 0.3 mm arranged in the tube wall. The active bending frame is processed by a precision 5-axis computer numerical control engraving machine. The passive bending part is a nine-chamber tube made of high-density polyethylene, which is produced through molds by vacuum cooling shaping.

TABLE I
Parameters Of The Active Bending Part

Parameters	Value
Length	32.4 mm
Outer diameter	2.8 mm
Inner diameter	1.2 mm
Number of the frames	17
Driven wire diameter	0.15 mm
Driven wire hole diameter	0.3 mm

In the case of using surgical forceps, the flexible instrument can provide 7 DOFs, including linear displacement, rotation,

shoulder pitch and yaw motions, wrist pitch and yaw motions, and opening and closing of surgical forceps. Each frame is connected and bended by driven wires with a maximum bending angle of 25°. Therefore, the maximum bending angle in both DOFs of shoulder is 50°, and the maximum bending angle in both DOFs of the wrist is 100°. Both the shoulder and wrist bending motions require two sets of 0.15 mm diameter multi-strand steel wires as driven wires.

In actual bending motion, if the displacement changes of the two driven wires for controlling the same bending degree are not equal, it is easy to cause two main problems: 1) deformation of the driven wires due to the tension brought by the tightened wires on both sides and 2) relaxation of the driven wire on one side. This will have a huge impact on the motion accuracy, flexibility, and service life of the flexible instrument. To solve this problem, the circular arc joint is designed for equal displacement changes of the driven wires. The model of the frame is shown in Fig. 2(a). The frames are contacted with each other by a well-fitting circular arc wall and circular arc joint.

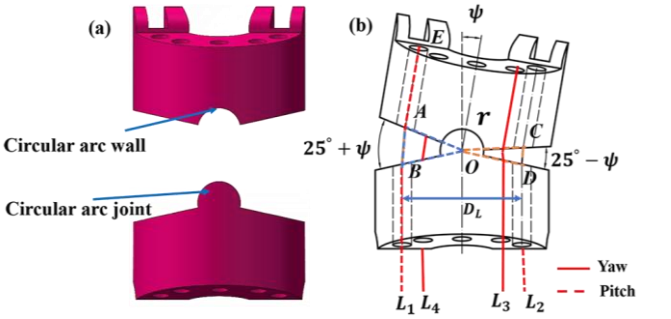

Fig. 2. Structure of the frame. (a) Model of the frame. (b) Deflection model of the frame.

The deflection model of the frame is shown in Fig. 2(b). The path of the driven wire can be divided into two parts. One part (AE) is the path through the driven wire hole inside the frame, which is equal for different driven wires and determined by the structural parameters of the frame itself. The other part is the distance between the corresponding driven wire holes among adjacent frames, that is, the chord length corresponding to the circle with O as the center and the line segment OA as the radius. The length of line segment OA is given by the structure of the frame, so the lengths of chords AB and CD are determined by the central angle corresponding to the chord, and changed with the variation of the frame deflection angle Ψ. Let $L1$ and $L2$ represent the path lengths of the driven wire determined by the chord length. It can be seen that $L1$ and $L2$ are functions of the frame deflection angle as the independent variable Ψ, and the lengths of the driven wire paths are determined by the following equations based on the geometrical relationships.

$$L_1 = D_L \sin(\frac{5\pi}{72} + \frac{\psi}{2}) \tag{1}$$

$$L_2 = D_L \sin(\frac{5\pi}{72} - \frac{\psi}{2}) \tag{2}$$

D_L is the distance between L_1 and L_2. When the angle is small, θ and $sin\theta$ have a good approximation relationship. Because the bending part adopts a discrete frame distribution stacking design, the maximum deflection angle of each frame is relatively small. Considering the maximum error at the limit bending position, that is, when the frame deflection angle is 25°, the relative error between θ and $sin\theta$ in (1) and (2) is only about 3%. Therefore, we can approximate (1) and (2) to obtain.

$$L_1 \approx D_L \cdot (\frac{5\pi}{72} + \frac{\psi}{2}) \tag{3}$$

$$L_2 \approx D_L \cdot (\frac{5\pi}{72} - \frac{\psi}{2}) \tag{4}$$

The displacement change of the left driven wire during the driven process is ΔL_1, and the displacement change of the right driven wire is ΔL_2. This can be easily obtained from equations (3) and (4).

$$|\Delta L_1| = |\Delta L_2| = D_L \cdot \frac{|\psi|}{2} \tag{5}$$

The proposed structure has the characteristic of approximately equal displacement changes of the driven wires in symmetrical positions. This ensures better smoothness of motion for the instrument.

B. Unfolding Structure and Decoupling Design

An unfolding structure that can form the surgical triangulation (Fig. 3(a)) is designed, as shown in Fig. 3.

The unfolding structure as shown in Fig. 3(b) consists of the shoulder active bending part and the elbow passively bending part, with 9 stacked frames in total, which can achieve an unfolding angle of 50° in the pitch and yaw directions.

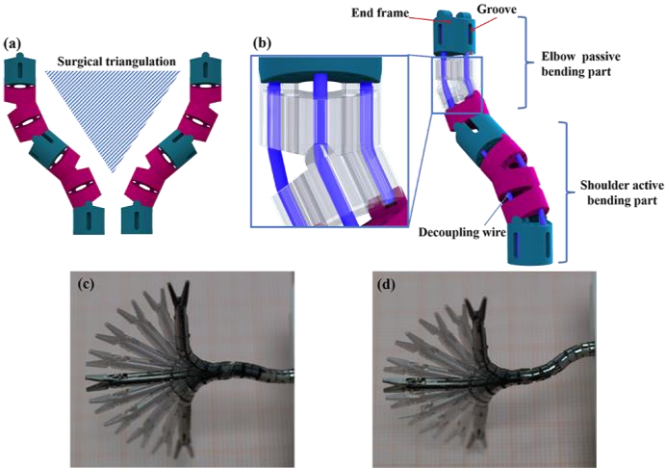

Fig. 3. 2-DOF unfolding design and pose of the unfolding state. (a) Surgical triangulation layout. (b) Decoupling design. (c) Shoulder bending in P-direction. (d) Shoulder bending in Y-direction.

The four decoupling wires used to form symmetrical constraints are arranged at the contacting circular arc joint positions. The decoupling wires with equal length are fixed at both ends in the grooves on the base and end frames. During the unfolding process, the frames of the elbow and shoulder undergo bending movements with equal angles but opposite directions because of the decoupling wires. This results in two beneficial outcomes: 1) the path length of the driven wire of

the entire unfolding structure remains unchanged, which solves the coupling between the unfolding structure and wrist part and 2) the orientation of the end frame of the unfolding structure connected to the wrist remains unchanged and parallel to the direction of the instrument channel, ensuring sufficient operating space for the instrument.

Fig. 3(c) and Fig. 3(d) show the bending behavior of the flexible instrument in the unfolding state, exhibiting good flexibility and verifying the decoupled design. The unfolding structure can remain stable without being affected by the bending of the wrist.

C. Kinematics Analysis

According to the continuum model [14] as shown in Fig. 4, it can be obtained from the geometric analysis:

$$d_{Li} = d_{L0}\cos(\alpha_B - \beta_i) \tag{6}$$

θ_B represents the bending angle, and α_B represents the twist angle. d_{L0} represents the distance from the driven wire hole to the neutral axis. d_{L1} represents the distance from the projection of the drive wire in the bending plane to the neutral axis. β_i $(i = 1,2,3,4)$ represent the position parameter of the drive wire hole, respectively. $\beta_1 = 57°$, and $\beta_1, \beta_2, \beta_3$ add $90°$ in sequence. The theoretical relationship between the displacement of the driven wire and the bending angle is obtained:

$$\Delta L_1 = -\Delta L_2 = -d_{L0}\theta_B\cos(\alpha_B - \beta_1) \tag{7}$$

$$\Delta L_3 = -\Delta L_4 = -d_{L0}\theta_B\sin(\alpha_B - \beta_1) \tag{8}$$

ΔL_i $(i = 1,2,3,4)$ represent the displacement of four driven wires, respectively.

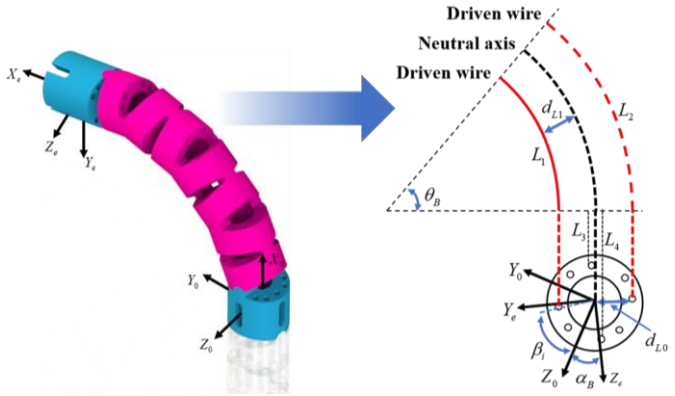

Fig. 4. Continuum model.

The frame coordinate system is shown in Fig. 5. The direction of the y-axis and z-axis is determined by the right-hand rule, assuming that each frame has the same rotation angle [15].

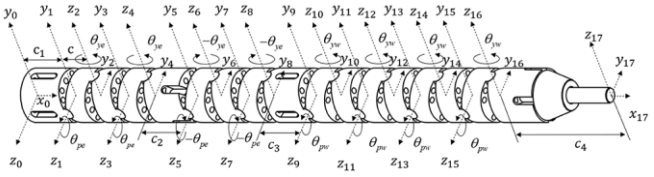

Fig. 5. Frame coordinate system.

The transformation matrix can be represented:

$$ {}^{i-1}_{i}\mathbf{T} = \begin{bmatrix} \cos\theta_i & -\sin\theta_i & 0 & a_{i-1} \\ \sin\theta_i\cos\alpha_{i-1} & \cos\theta_i\cos\alpha_{i-1} & -\sin\alpha_{i-1} & -\sin\alpha_{i-1}d_i \\ \sin\theta_i\sin\alpha_{i-1} & \cos\theta_i\sin\alpha_{i-1} & \cos\alpha_{i-1} & \cos\alpha_{i-1}d_i \\ 0 & 0 & 0 & 1 \end{bmatrix} \tag{9}$$

D-H parameter method with Craig's convention is used to obtain the corresponding parameters. Then, the transformation matrix between the end effector coordinate system and the base coordinate system is obtained.

$$ {}^{0}_{17}T = \prod_{i=1}^{17} {}^{i-1}_{i}T = \begin{bmatrix} \mathbf{R} & \mathbf{p} \\ 0 & 1 \end{bmatrix} = \begin{bmatrix} n_x & s_x & a_x & p_x \\ n_y & s_y & a_y & p_y \\ n_z & s_z & a_z & p_z \\ 0 & 0 & 0 & 1 \end{bmatrix} \tag{10}$$

$\mathbf{p} = [p_x, p_y, p_z]$ provides the end pose of the flexible instrument. $\mathbf{R}$ reflects the spatial pose of the flexible surgical instrument. Based on this, theoretical analysis of the workspace can be carried out. The working space is plotted using the Monte Carlo interpolation method in MATLAB, and the result is shown in Fig. 6.

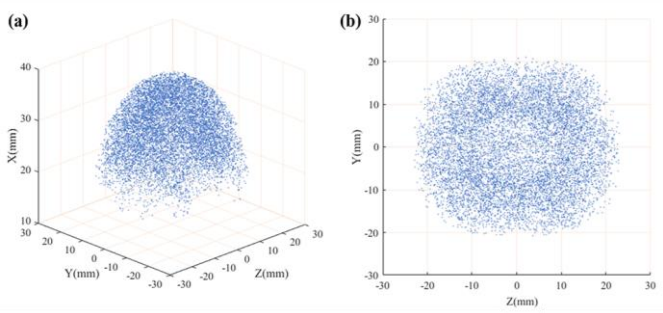

Fig. 6. Workspace of the flexible instrument. (a) 3-D view. (b) Y-Z view.

D. End Effector and Actuation Unit

A surgical forceps has been designed, as shown in Fig. 7(a). It consists of two jaws, a fixed pin, a sliding pin, a driving slider, and a reset spring. The maximum external diameter when closed is consistent with the flexible instrument that is 2.8mm. The maximum length is 12.5mm, and the maximum opening angle is 60°. The structure of the monopolar high-frequency electric knife is shown in Fig. 7(b).

The overall structure of the actuation unit is shown in Fig. 6(c). It includes three main parts: 1) linear actuation unit based on the screw guide transmission, 2) rotation actuation unit with synchronous belt transmission, and 3) end effector and bending actuation unit with wire rolling mechanism. The motor selected is a miniature brushless DC motor (1226S012B, Faulhaber, German), with a reduction ratio of 879:1.

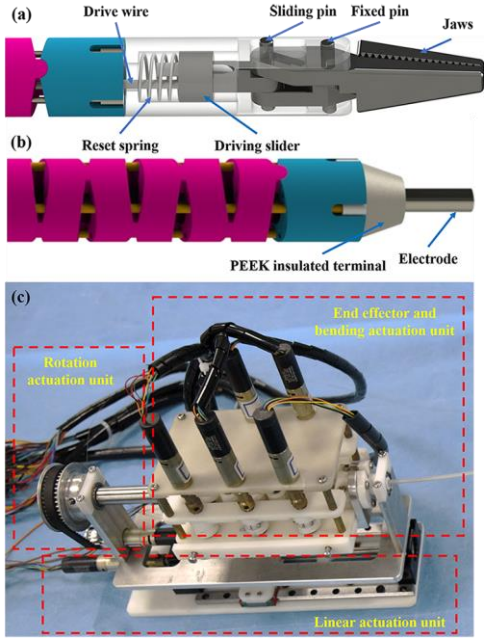

Fig. 7. (a) Structure of the surgical forceps. (b) Structure of the electric knife. (c) Actuation unit.

E. Mater-slave Control Method

The haptic device (Omega.6, Force Dimension, Switzerland) is selected as master operator. The position and angle information of the master operator are mapped to the linear displacement and the wrist bending of the flexible instrument, as shown in Fig. 8.

Fig. 8. Mapping relationship in master-slave control.

The proportional master-slave mapping can be expressed as:

$$\begin{cases} k_x \cdot x_{master} = l_s \\ k_{sy} \cdot y_{master} = \theta_{sy} \\ k_{sz} \cdot z_{master} = \theta_{sp} \\ k_{wy} \cdot \theta_z = \theta_{wy} \\ k_{wz} \cdot \theta_y = \theta_{wp} \\ k_r \cdot \theta_x = \theta_r \end{cases} \tag{11}$$

$x_{master}, y_{master}, z_{master}, \theta_x, \theta_y, \theta_z$ represent the linear displacement and rotation angle of the master operator in three directions. $\theta_{sy}, \theta_{sp}, \theta_{wy}, \theta_{wp}$ represent the bending angles in yaw and pitch directions of the wrist and the shoulder, respectively. l_s, θ_r represent the linear displacement and the rotation angle of the instrument, respectively. $k_{sy}, k_{sz}, k_{wy}, k_{wz}, k_x, k_r$ represent the proportional factors of the bending angles in yaw and pitch directions of the wrist and shoulder, linear displacement and rotation angle, respectively. We used the button on the master operator handle to control the opening and closing of the surgical forceps. In the actual use, the shoulder part of the instrument is primarily meant to establish the surgical triangulation. Therefore, once it's positioned at the appropriate angle, its location can be fixed to prevent the occurrence of motion coupling in the master-slave control. The time delay of the instrument from the receipt of a command to its completion is less than 20 ms that makes the operator hardly feel the delay.

III. Results

A. Wrist Workspace Evaluation

During the surgical procedure, the elbow and shoulder bending parts of the flexible instrument is in a specific unfolding state and remains stable. Therefore, we evaluated the working space of wrist bending part separately.

The motion of the flexible instrument was captured and recorded using a binocular vision sensor (Polaris, NDI, Canada). The marker was placed at the end of the instrument. The actual test workspace is compared with the theoretical workspace that is calculated using D-H method, as shown in Fig. 9. The actual test result indicates that the instrument can cover a hemi-spherical workspace up to 24 mm in radius, and the actual test result is consistent with the theoretical result.

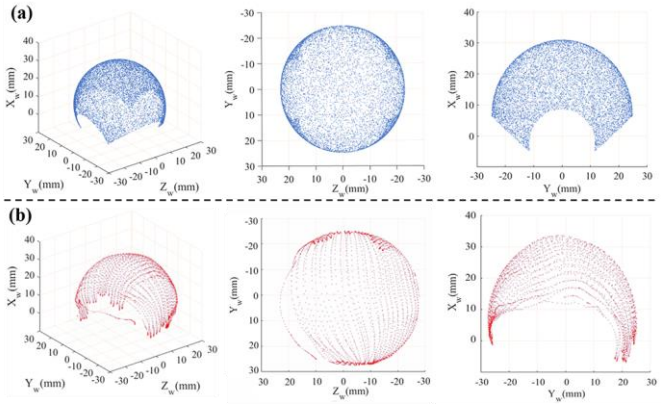

Fig. 9. Wrist workspace. (a) Theoretical workspace. (b) Actual workspace.

B. Rotation Evaluation

Flexible instrument can achieve a ±90° rotating motion. Rotation tests were conducted on the rotational angle, and the results that the instrument rotated from -90° to 90° are shown in Fig. 10. The strip-shaped object fixed at the end of the forceps (indicated by the red line) indicates the rotational angle.

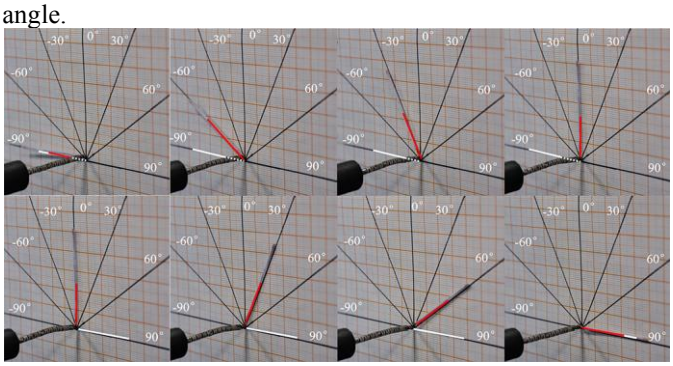

Fig. 10. Rotation angle test.

C. Loading Evaluation

Loading tests were conducted on both the clamping force and manipulating force of the flexible instrument. A thin film pressure sensor (RP-C5-ST-LF5, K-CUT, China) was used to test the clamping force. The result for the clamping force is shown in Fig. 11.

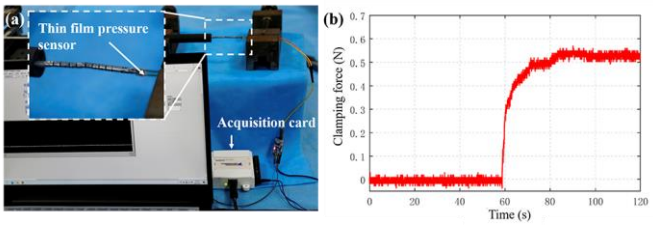

Fig. 11. (a) Setup for the clamping force test of the gripper. (b) Result for the clamping force.

Fig. 12 shows the results of the manipulating force. We used weights of 0.1 N, 0.2 N, 0.5 N, 0.7 N, 1 N, and 1.2 N as loads on the bending part. The results indicate that the instrument can lift a load of 0.7 N and still maintain its shape stability. The maximum lifting load is about 1 N with shape deformation.

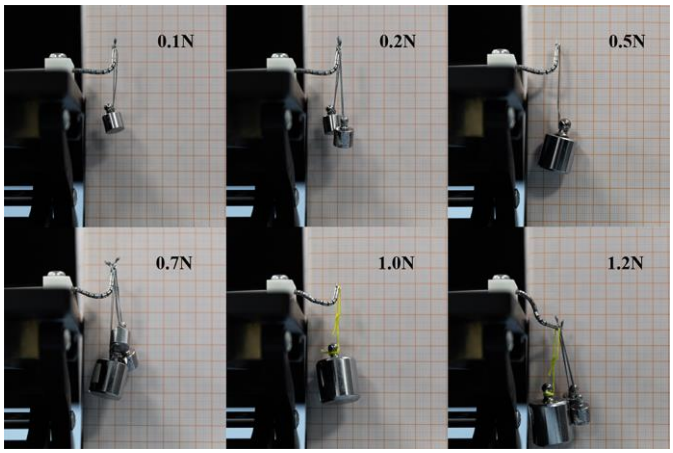

Fig. 12 Loading test of bending part.

D. Motion Accuracy Evaluation

We have tested the wrist bending motion of the flexible instrument in three different states including without unfolding, shoulder bending in pitch-direction (P-direction) and shoulder bending in yaw-direction (Y-direction). The bending angle was recorded with a camera. We repeated the experiment five times.

The theoretical value was calculated according to equations (7) and (8). The experimental results with the wrist bending motion in three different unfolding states are shown in Fig. 13.

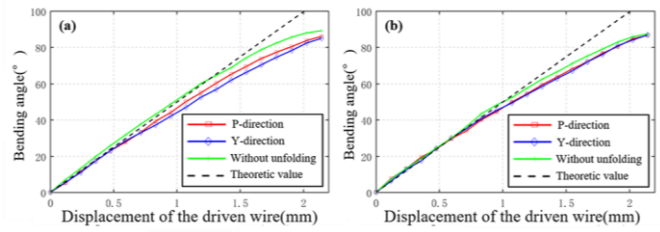

Fig. 13. (a) Bending test of wrist in pitch direction. (b) Bending test of wrist in yaw direction.

Based on the analysis of the above results, there is an approximate linear relationship between the wrist bending angle and the wire displacement in all three states. Moreover, at small angles (less than 40°), there is excellent consistency with the continuum model. As the bending angle increases, the deviation between the experimental data and the continuum model gradually increases, especially during the unfolding of the instrument, which results in a maximum error of about 16% compared to the theoretical value. The measured values of bending repeatability error (root mean square error, RMSE) and tip positioning accuracy (calculated by the product of wrist length and RMSE) are presented in Table II.

TABLE II
RESULTS OF MEASUREMENT IN BENDING MECHANISM

Measurement item	Without unfolding	P-direction	Y-direction
Repeatability error (°)	1.38	1.29	2.29
Tip positioning accuracy (mm)	0.35	0.33	0.59

E. In-vivo Animal Trial

To fully verify the flexibility and reliability of the flexible instrument, *in-vivo* animal trail was carried out. The set up of the experiment is shown in Fig. 14. The flexible instrument is carried into the target position of the swine rectum via an endoscopic platform developed previously. The master operators use two haptic devices (Omega.6) to control the electric knife and surgical forceps respectively. A swine (male, 60kg) was under general anesthesia throughout the experiments. This animal trial was reviewed and approved by the Ethics Committee of Teda International Cardiovascular Hospital (Approval #: TICH-JY-202205027-4).

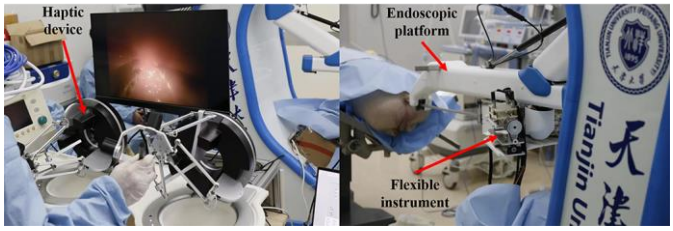

Fig. 14. Set up of *in-vivo* animal trails.

The ESD result is shown in Fig. 15. First, the endoscope platform is controlled to insert into the target position of the rectum. Second, a disposable endoscopic injection needle is used to inject the staining solution under the mucosa in the target area, while separating the mucosa. Afterwards, the electric knife and surgical forceps are used to perform surgical procedure on the simulated target area. The electric knife was firstly adopted to pre-cut the mucosa and its underlying layers until a large gap was cut out that can be grasped by forceps. After that, the forceps was used to pull and lift the mucosa to expose the cutting edge. With the assistance of forceps, electric knife can strip the mucosa easily. The procedure was performed until the mucosa was completely cut off. Finally, the endoscopic platform was withdrawn to take out the peeled mucosal sample. The size of the dissection area reached 180 mm^2. The system was operated smoothly without any malfunction during the procedure. There were no incidents of perforation or significant bleeding during the surgery.

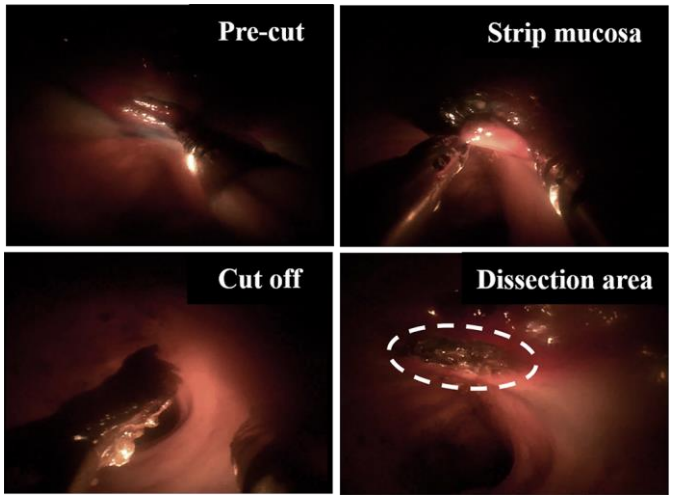

Fig. 15. *In-vivo* animal ESD.

IV. Discussion

This work proposes a new type of multi-DOFs flexible instrument, to address the limitations of current robotic flexible instruments, including their large size, poor flexibility and triangulation, and coupling of multi-segment bending. The instrument is equipped with forceps and a high-frequency electric knife as its end effectors, enabling it to perform ESD procedure. As shown in Table III, the instruments [12, 16-18] also adopt discrete frame stacking structure to increase the motion accuracy and stability. However, they have a large outer diameter with over 3 mm that can't satisfy the space of the mainstream GI endoscope. And they have a maximum of 5 DOFs, which is less than the instrument proposed in this paper. STRAS [19] has the end-tip mechanism for surgical triangulation, but only one DOF is difficult to meet the ESD needs. ViaCath [20] has two distal bending parts, but there is coupling between them so as to affect the motion accuracy. With the decoupling design, the wrist and shoulder of the instrument proposed in this paper can bend independently to form operation triangulation and countertraction effectively.

TABLE III
Comparison Of Different Instruments

Surgical instrument	Outer diameter (mm)	DOF	Surgical triangulation	Decoupling design
I^2 snake [12]	3.8	5	No	No
K-FLEX [16]	3.7	4	No	No
DDES [17]	4.0	5	No	No
FLEX [18]	3.5	2	No	No
STRAS [19]	3.5	1	Yes	No
ViaCath [20]	4.75	4	Yes	No
This work	2.8	6	Yes	Yes

A double bending structure is developed, including 2 DOFs unfolding structure and 2 DOFs wrist bending structure, which can expand working space and realize surgical triangulation. At the same time, a decoupling design based on the symmetrical unfolding structure is realized. The flexible instrument can achieve a hemi-spherical workspace with a radius of 24 mm without considering linear movement.

Through optical tracking, recording, and 3D reconstruction of the workspace of the wrist bending part, the result consisted with the theoretical workspace. In addition, from the 3-D view and X-Y view of the workspace, it can be seen that at positions with larger bending angles, the actual test range is smaller than the theoretical result. This is due to the deformation of the driven wire under heavy load at large bending angles, resulting in a decrease in the bending angle. In the actual use, this problem can be solved by appropriately adjusting the master-slave proportional factors.

The rotation of the flexible surgical instrument was tested, achieving a motion range of ±90°. From the experimental results, it can be seen that the instrument can maintain a stable pose at a specific angular position. The gripping force of the forceps and the load capacity of the bending part were tested and evaluated. The test result indicated that the forceps can provide a clamping force of approximately 0.53 N, which should be enough to clamp mucosal sample and take it out. The flexible instrument can withstand a maximum load of 1 N, which can also meet the gastrointestinal endoscopic surgical requirements [21]. In endoscopic procedure, energy instruments such as electric knife are mainly used that does not require large manipulating force. The endoscopic forceps are used for biopsy or lifting mucosal layers (under 2 mm in thickness). A load capacity of 1N can meet the needs of the procedure, which is also proven by the *in-vivo* animal trial. Through bending experiments of the wrist, it has been proven that the motion of the wrist bending part approximates the continuum model, with a maximum error of about 16%. The possible reason is that the path of the driven wire changes from a straight line to a curved shape after unfolding, which increased friction with the driven wire of the wrist, resulting in driven wire's noticeable creep. The RMSEs without unfolding, with shoulder bending in P-direction and with shoulder bending in Y-direction are 1.39°, 1.29°and 2.29°, respectively. Tip positioning accuracy without unfolding, with unfolding in P-direction and with unfolding in Y-direction is 0.353 mm, 0.329 mm and 0.585 mm, respectively. *In-vivo* animal trial has verified that the instrument's motion accuracy is sufficient to perform ESD successfully.

In vivo animal trial on ESD was carried out. After 92 minutes, a 180 mm^2 dissection area was successfully cut out. Through master-slave operation, the complexity of surgery can be reduced, and the learning curve of doctors can be optimized. No perforation or System fault occurred during the procedures. Postoperative examination of the resection area did not find bleeding. The collaborating endoscopist (operator) commented that with the assistance of this instrument, ESD has become easier and less fatiguing. Due to the use of an intuitive master-slave control method, the learning curve has also significantly decreased.

In clinical scenarios, Digestive tract peristalsis may affect the progress of the surgery. Adopting motion compensation technology and use of drugs to reduce peristalsis could be considered to solve this issue. Blood and intestinal tissues

may also enter into the gaps of frames that could affect the bending movement of instrument. A thin coating can be covered on the outside of instrument to prevent this situation.

V. Conclusion

In this study, we have developed a novel miniature flexible instrument to address the problems associated with limited flexibility and surgical triangulation in endoscopic procedure. Compared to other robotic flexible instruments, it has a smaller outer diameter and more DOFs. Experimental results have shown that the instrument has a large hemi-spherical workspace and high motion accuracy. *In-vivo* animal trial has demonstrated that the instrument can successfully perform ESD and has high clinical potential for GI endoscopic procedures.

VI. Acknowledgement

The authors would like to thank Dr. Xin Chen and Dr. Bo Wei for assisting and discussion for *in-vivo* animal trial.

References

[1] F. Bray, J. Ferlay, I. Soerjomataram, R. L. Siegel, L. A. Torre, and A. Jemal, "Global cancer statistics 2018: GLOBOCAN estimates of incidence and mortality worldwide for 36 cancers in 185 countries," *CA: a cancer journal for clinicians,* vol. 68, no. 6, pp. 394-424, 2018.

[2] M. Luo and L. Li, "Clinical utility of miniprobe endoscopic ultrasonography for prediction of invasion depth of early gastric cancer: A meta-analysis of diagnostic test from PRISMA guideline," *Medicine,* vol. 98, no. 6, 2019.

[3] S. Zuo and S. Wang, "Current and emerging robotic assisted intervention for NOTES," *Expert review of medical devices,* vol. 13, no. 12, pp. 1095-1105, 2016.

[4] T. Kato, I. Okumura, H. Kose, K. Takagi, and N. Hata, "Tendon-driven continuum robot for neuroendoscopy: validation of extended kinematic mapping for hysteresis operation," *International journal of computer assisted radiology and surgery,* vol. 11, pp. 589-602, 2016.

[5] Z. Ping, T. Zhang, L. Gong, C. Zhang, and S. Zuo, "Miniature flexible instrument with fibre bragg grating-based triaxial force sensing for intraoperative gastric endomicroscopy," *Annals of Biomedical Engineering,* vol. 49, pp. 2323-2336, 2021.

[6] A. Gao, H. Liu, Y. Zou, Z. Wang, M. Liang, and Z. Wang, "A contact-aided asymmetric steerable catheter for atrial fibrillation ablation," *IEEE Robotics and Automation Letters,* vol. 2, no. 3, pp. 1525-1531, 2017.

[7] A. Schmitz, S. Treratanakulchai, P. Berthet-Rayne, and G.-Z. Yang, "A rolling-tip flexible instrument for minimally invasive surgery," in *2019 International Conference on Robotics and Automation (ICRA)*, 2019, pp. 379-385: IEEE.

[8] C. Min Seow, W. Jian Chin, C. A. Nelson, A. Nakamura, S. M. Farritor, and D. Oleynikov, "Articulated manipulator with multiple instruments for natural orifice transluminal endoscopic surgery," *Journal of Medical Devices,* vol. 7, no. 4, 2013.

[9] F. Van Meer, A. Giraud, D. Esteve, and X. Dollat, "A disposable plastic compact wrist for smart minimally invasive surgical tools," in *2005 IEEE/RSJ International Conference on Intelligent Robots and Systems*, 2005, pp. 919-924: IEEE.

[10] K. Harada, K. Tsubouchi, M. G. Fujie, and T. Chiba, "Micro manipulators for intrauterine fetal surgery in an open MRI," in *Proceedings of the 2005 IEEE International Conference on Robotics and Automation*, 2005, pp. 502-507: IEEE.

[11] W. Hong, A. Schmitz, W. Bai, P. Berthet-Rayne, L. Xie, and G.-Z. Yang, "Design and compensation control of a flexible instrument for endoscopic surgery," in *2020 IEEE International Conference on Robotics and Automation (ICRA)*, 2020, pp. 1860-1866: IEEE.

[12] P. Berthet-Rayne *et al.*, "The i 2 snake robotic platform for endoscopic surgery," *Annals of biomedical engineering,* vol. 46, pp. 1663-1675, 2018.

[13] X. Zhang, S. Elkoun, A. Ajji, and M. Huneault, "Oriented structure and anisotropy properties of polymer blown films: HDPE, LLDPE and LDPE," Polymer, vol. 45, no. 1, pp. 217-229, 2004.

[14] R. J. Roesthuis and S. Misra, "Steering of multisegment continuum manipulators using rigid-link modeling and FBG-based shape sensing," IEEE transactions on robotics, vol. 32, no. 2, pp. 372-382, 2016.

[15] J.-w. Suh, K.-y. Kim, J.-w. Jeong, and J.-j. Lee, "Design considerations for a hyper-redundant pulleyless rolling joint with elastic fixtures," IEEE/ASME Transactions on Mechatronics, vol. 20, no. 6, pp. 2841-2852, 2015.

[16] M. Hwang and D. S. Kwon, "K‐FLEX: a flexible robotic platform for scar‐free endoscopic surgery," The International Journal of Medical Robotics and Computer Assisted Surgery, vol. 16, no. 2, p. e2078, 2020.

[17] C. C. Thompson, M. Ryou, N. J. Soper, E. S. Hungess, R. I. Rothstein, and L. L. Swanstrom, "Evaluation of a manually driven, multitasking platform for complex endoluminal and natural orifice transluminal endoscopic surgery applications (with video)," Gastrointestinal endoscopy, vol. 70, no. 1, pp. 121-125, 2009.

[18] P. J. Schuler, T. K. Hoffmann, U. Duvvuri, N. Rotter, J. Greve, and M. O. Scheithauer, "Demonstration of nasopharyngeal surgery with a single port operator‐controlled flexible endoscope system," Head & Neck, vol. 38, no. 3, pp. 370-374, 2016.

[19] F. Nageotte, L. Zorn, P. Zanne, and M. De Mathelin, "Stras: A modular and flexible telemanipulated robotic device for intraluminal surgery," in Handbook of robotic and image-guided surgery: Elsevier, 2020, pp. 123-146.

[20] D. J. Abbott, C. Becke, R. I. Rothstein, and W. J. Peine, "Design of an endoluminal NOTES robotic system," in 2007 IEEE/RSJ International Conference on Intelligent Robots and Systems, 2007, pp. 410-416: IEEE.

[21] T. Ranzani et al., "A novel device for measuring forces in endoluminal procedures," International Journal of Advanced Robotic Systems, vol. 12, no. 8, p. 116, 2015.